Dyes and Pigments 223 (2024) 111957

Contents lists available at ScienceDirect

Dyes and Pigments

journal homepage: www.elsevier.com/locate/dyepig

A PEGylated star polymer with a silver-porphyrin core as an efficient photo-antimicrobial agent

Fabiana Vento [a], Angelo Nicosia [a], Lidia Mezzina [a], Domenico Franco [b], Roberto Zagami [b], Antonino Mazzaglia [c], Placido Giuseppe Mineo [a,d,*]

[a] Department of Chemical Sciences and INSTM UdR of Catania, University of Catania, V.le A. Doria 6, 95125 Catania, Italy
[b] Department of Chemical, Biological, Pharmaceutical and Environmental Sciences, University of Messina, V.le F. Stagno D'Alcontres 31, 98166 Messina, Italy
[c] National Council of Research, Institute for the Study of Nanostructured Materials (CNR-ISMN), URT of Messina C/o Department of Chemical, Biological, Pharmaceutical and Environmental Sciences, University of Messina, V.le, F. Stagno D'Alcontres, 31, 98166 Messina, Italy
[d] CNR-IPCF Istituto per I Processi Chimico-Fisici, Viale F. Stagno D'Alcontres 37, I-98158 Messina, Italy

ARTICLE INFO

Keywords:
Antibacterial activity
PEGylated porphyrin
Pseudomonas aeruginosa
Staphylococcus aureus
Silver-porphyrins
Photodemetallation

ABSTRACT

Antibacterial agents play a pivotal role in healthcare to prevent contamination of biomedical devices, which can determine infections in surgical and traumatic wound treatments. Furthermore, the COVID-19 pandemic has amplified the importance of protecting common surfaces to avoid bacterial contamination issues. Phenomena such as bacterial resistance push research to develop innovative antibacterial nanosystems. In this context, various agents showing antibacterial properties have appeared, including drug-releasing polymers, organic/inorganic hybrids, and porphyrin derivatives. The silver-based porphyrin derivatives show antibacterial properties despite having some drawbacks, such as toxicity for humans. On the other hand, water-soluble porphyrins, obtained by functionalization of the porphyrin core with PEG chains that enhance solubility and provide stealth properties, have gained attention because of their biocompatibility, structural stability, and tunability. This study focuses on the synthesis and characterization of a PEGylated silver-porphyrin that shows photo-activated antibacterial properties against *Pseudomonas aeruginosa* and *Staphylococcus aureus,* antibiotic-resistant pathogens that often coexist and contribute to biofilm-related problems. The porphyrinic system was characterized through NMR, UV–Vis, and fluorescence spectroscopies. Its in-vitro antibacterial activity was investigated and compared with that of the metal-free counterpart. To elucidate the influence of the complexed silver ion and its free base on the photo-antimicrobial effect, the occurrence of demetallation phenomena under irradiation was investigated. The experimental data suggest that the complexation of the silver ion protects the porphyrin core, allowing the photo-bactericidal activity of the system through photo-demetallation phenomena under light irradiation.

1. Introduction

Antibacterial agents are fundamental in the healthcare system to avoid contamination of biomedical products, which often leads to infection in the treatment of surgical and traumatic wounds [1]. The appearance of phenomena such as the development of bacterial resistance [2], points to the usefulness of the increasing efforts in the design of antibacterial-oriented molecules and nanomaterials. In addition to the need for antibacterial agents for biomedical devices and healthcare products, the importance of these agents has increased steadily after the recent COVID-19 pandemic scenario. Indeed, it is important to provide adequate protection for common surfaces, since contamination by bacteria could produce a protective biofilm that can be also colonized by different viruses, becoming an efficient diffusion pathway [3].

Among the most prevalent bacteria species, *Pseudomonas aeruginosa (P. aeruginosa)* and *Staphylococcus aureus (S. aureus*) are ubiquitous pathogens [4,5]. These are a common cause of infections, also acting synergistically [6], and have been related to most biofilm-associated clinical issues [7]. *P. aeruginosa* usually colonizes the surface of biomedical devices, while *S. aureus*, despite its close relationship with the human microbiota, could also induce several diseases [8]. Moreover, even though they follow different biological pathways, both have shown the ability to develop antibiotic resistance [4,9]. In this context, when attempting to develop an antibacterial agent, it is important to avoid the

* Corresponding author. Department of Chemical Sciences and INSTM UdR of Catania, University of Catania, V.le A. Doria 6, 95125 Catania, Italy.
E-mail address: gmineo@unict.it (P.G. Mineo).

https://doi.org/10.1016/j.dyepig.2024.111957
Received 31 October 2023; Received in revised form 7 December 2023; Accepted 9 January 2024
Available online 14 January 2024

use of antibiotics, in addition to providing broad-spectrum antibacterial activity [2].

In recent years, several kinds of material possessing antibacterial properties have been developed, including drug-releasing bioabsorbable polymers [10], organic/inorganic hybrid systems [11], and metal-based products [12]. For instance, metal ions, such as silver, show microbicidal activity at low concentrations, but their effectiveness comes with the drawback of being extremely toxic when their concentration exceeds certain thresholds [13,14]. More recently, dyes able to provide photosensitized antibacterial activity, such as porphyrins [15], have attracted considerable attention due to their good biocompatibility, stable structure, and useful macrocycle modification [16]. The chemical-physical properties of porphyrins are strongly influenced by their chemical composition and substituents, so these could be easily tuned: as an example, by introducing suitable functional groups that increase the lipophilicity of the macromolecular system, it is possible to favor the penetration into the lipid membrane [17] and interfere with the normal activity of the bacteria [18]. Although much attention has been paid to the use of free-base ionic porphyrins, metalloporphyrins [19] or their supramolecular systems [20,21] have shown low toxicity and are capable of treating different infections using a large number of mechanisms [22].

Among all metalloporphyrins reported in the literature, those functionalized with PEG have shown peculiar properties due to the presence of PEG chains that, covalently bound to the porphyrin core, promote its solubility in the biological environment [23–26]. Moreover, PEG chains are well known to give stealth properties to the porphyrin core [27,28] ensuring a higher circulation time in the body during therapeutic administration. This, combined with the ability of porphyrins to produce reactive singlet oxygen, makes these systems also suitable for applications in photodynamic therapy [17,29]. Aiming to investigate on the potentialities of polymer-based antibacterial agents, in this work a PEGylated silver-porphyrin system having four PEG chains covalently linked to the porphyrin macrocycle ($AgP4PEG_{750}$) has been synthesized and suitably characterized through MALDI-TOF spectrometry and NMR, UV–Vis and fluorescence spectroscopies. Photoirradiation experiments in water solution were performed to investigate the photo-demetallation pathway of the porphyrin derivative. The *in-vitro* antibacterial activity was investigated against *P. aeruginosa* and *S. aureus,* and compared with that of its metal-free counterpart to understand the influence of the complexed silver ion on its photoantimicrobial effect.

2. Material and methods

2.1. Reagents

All solvents and basic materials were commercial products (Sigma-Aldrich). *Pseudomonas aeruginosa* ATCC27853 and *Staphylococcus aureus* ATCC29213 were purchased from the American Type Culture Collection (LGC Promochem, Milan, Italy) and cultured in Luria-Bertani broth (LB, Sigma-Aldrich, Milan) and tryptone soy broth (TSB, Sigma-Aldrich, Milan), respectively. Both bacterial strains were maintained in their respective media supplemented with 20 % glycerol at −80 °C.

2.2. 5,10,15,20-[p-(ω-methoxy-polyethyleneoxy) phenyl] porphyrin synthesys

The 5,10,15,20-[*p*-(ω-methoxy-polyethyleneoxy) phenyl] porphyrin (H_2P4PEG_{750}) was obtained as previously described [30–32]. Briefly, by etherification reaction between 5,10,15,20-tetrakis (*p*-hydroxyphenyl) porphyrin (P) and chlorinated poly (ethylene glycol) methyl ether ($PEGMEC_{750}$), a mixture of mono, di, tri and tetra functionalized porphyrin derivatives were produced. In a 25 mL flask, 1 g (2.86 mmol) of PEGMEC-750 was dissolved in an H_2O/THF 1:1 mixture (12 mL), then, 0.24 g (0.354 mmol) of P was dissolved in 2.84 mL of sodium hydroxide 0.5 M aqueous solution. The two solutions were mixed and refluxed for 76 h. The reaction product was acidified with acetic acid and dried under vacuum at 80 °C for 24 h. The residue was dissolved in chloroform and fractionated into its components by means of column chromatography using silica gel as the stationary phase and a solution of $CHCl_3/C_2H_5OH/(C_2H_5)_3N$ (97:2:1) as eluent. 5,10,15, 20-[*p*-(ω-methoxy-polyethyleneoxy) phenyl] porphyrin H_2P4PEG_{750} corresponding to the first chromatographic eluted band, was obtained with a yield of about 30 % with respect to the initial porphyrin amount.

2.3. $AgP4PEG_{750}$ synthesis

$AgP4PEG_{750}$ was synthesized as reported elsewhere [33,34] and opportunely modified. Briefly, 1.45 mg (4×10^{-7} mol) of H_2P4PEG_{750} and 118 mg of $AgNO_3$ (0.7 mmol), solubilized in 2.5 mL of water, were sonicated for 30 min and kept under stirring for 24 h. The reaction product was dried with an N_2 stream. The so-obtained metallated porphyrin was separated from the unreacted reagents through chromatographic separation, using silica gel as the stationary phase and a solution of CH_2Cl_2/MeOH (9:1) as eluant. The first coloured band, corresponding to $AgP4PEG_{750}$, was dried with N_2 and kept in a vacuum oven (50 °C, 24 h) with a yield of about 70 % with respect to the initial H_2P4PEG_{750} amount.

2.4. Bacteria strain, media and growth conditions

Antibacterial tests were carried out by increasing aliquots of each specimen, namely H_2P4PEG_{750} and $AgP4PEG_{750}$, up to 25 μM. For each strain, a semi-exponential broth culture was prepared at a final concentration of about 10^5 bacteria/mL starting from 0.5 Mc Farland inoculum (~1.5×10^8 bacteria/mL). Then, 200 μL of bacterial suspension were aliquoted in wells of 96-well plate (3 replicates per condition) and incubated under a white-light source (26,000 lux, fluence rate 3.81 mW/cm^2) for 4 h (totalling 54.82 J/cm^2 fluence). After light irradiation, the plates were incubated in the dark for 18 h at 37 °C and the bacterial growth was verified spectrophotometrically at optical density 540 nm (OD_{540}). To detect any bactericidal activity due to non-irradiated compounds, control plates were prepared in the same conditions but kept in the dark for the entire incubation period. Minimum bactericidal concentration (MBC) was determined by subculturing in fresh medium from each well without any visible growth and defined as the lowest concentration of compound able to reduce bacterial viability by over 99.9 % with respect to the initial inoculum. The viable bacteria were quantified by Colony Forming Unity (CFU) assay and expressed as bacterial viability percentage compared to a positive control (bacterial culture without compounds) [35]. For ANOVA test from Tukey's multiple comparisons test, one (*), two (**) and three (***) asterisks identify p-value <0.05, 0.01 and 0.001, respectively. For each point, the mean and standard deviation were derived from 3 experimental data.

Medium, reagent and tested compounds were evaluated after saturated steam sterilization (121 °C, 20').

2.5. Characterization methods

UV–Vis spectra were recorded on a Cary 60 UV–Vis spectrophotometer (Agilent Technologies, Santa Clara, CA, USA) using PMMA cuvettes (1 cm path length) and water as solvent.

Fluorescence spectra were acquired with a FP-8200 spectrofluorimeter (Jasco Corporation, Tokyo, Japan), in PMMA cells (1 cm path length), using water as a solvent (T = 25.0 ± 0.1 °C). The UV–Vis and fluorescence spectra were processed using the software "Spectragryph - optical spectroscopy software" (version 1.2.16.1, 2022, https://www.effemm2.de/spectragryph).

MALDI-TOF mass spectra were acquired with a Voyager DE (PerSeptive Biosystem, PerkinElmer, Waltham, MA, USA), detective the positive ions in linear mode by using the delay extraction device (25 KV applied after 2600 ns, a potential gradient of 454 V mm^{-1} and a wire

voltage of 25 V) [36,37]. The instrument calibration was performed as previously reported [38]. Average molecular weights were determined using Grams/386 software (Version 3.04, Galactic Industries Corp), through a suitable method [39].

3. Results

3.1. Syntheses and structural characterization

The 5,10,15,20-[*p*-(ω-methoxy-polyethyleneoxy) phenyl] porphyrin (H_2P4PEG$_{750}$) has been synthetized by etherification reaction (Scheme 1, Step 1) between 5,10,15,20-tetrakis (*p*-hydroxyphenyl) porphyrin (P) and poly (ethylene glycol) methyl ether chloride (PEGMEC$_{750}$) [31]. The H_2P4PEG$_{750}$ compound was isolated through column chromatography (first collected bands), and the chemical structure was confirmed through ^{1}H NMR spectroscopy and MALDI-TOF mass spectrometry.

The ^{1}H NMR of H_2P4PEG$_{750}$ shows the following signals (Fig. S1): a singlet at 8.90 ppm (8 H, *C*–H pyrrole protons), two doublets at 8.13 ppm (8 H, *C*–H phenyl protons γ with respect to the phenolic oxygen, *a*) and 7.32 ppm (8 H, *C*–H phenyl protons α with respect to the phenolic oxygen, *b*), two unresolved triplets centered at 4.42 and 4.02 ppm (for a total of 16 H, CH_2 groups of the first repetitive unit of PEG bind to porphyrin, *c* and *d*), an unresolved multiplet between 3.85 and 3.43 ppm (about 272 H, the methylene groups of the PEG arms, *PEG*), few singlets between 3.33 and 3.30 ppm (12 H, the –OCH_3 terminal groups of the branches, *ω*), a singlet at −2.80 ppm (2 H, *N*–H pyrrole protons, *21, 22*). The residual signal of the solvent CD_2Cl_2 is at 5.32 ppm.

The mass spectrum of H_2P4PEG$_{750}$ (Fig. 1a) shows a cluster of peaks centered at about 3450 Da ($\overline{Mn}$ = 3440 Da, $\overline{Mw}$ = 3600 Da), with two distributions of peaks each at *m/z* values of "2914 + *n* 44" and "2930 + *n* 44" corresponding to the [M]Na^+ (#) and [M]K^+ (*) species, respectively.

To obtain the silver-porphyrin, the metalation of the H_2P4PEG$_{750}$ was carried out using an aqueous solution of silver nitrate (see Scheme 1, Step 2, and the experimental section) at room temperature [40]. To isolate the 5,10,15,20-[p-(ω-methoxy-polyethyleneoxy) phenyl] silver porphyrin (AgP4PEG$_{750}$) from the nitrate silver salts, the reaction product was purified through column chromatography, collecting only the first coloured band. Unfortunately, due to the paramagnetic nature of AgP4PEG$_{750}$, an optimal ^{1}H NMR spectrum was not obtained (spectrum not shown). Nevertheless, as evidence of the insertion of silver ions into the tetrapyrrolic cavity, the disappearance of the signal at −2.78 ppm (typical of NH groups present in the pyrrolic core) was ascertained.

Moreover, Ag^{II} ion insertion into the porphyrin core was confirmed through MALDI-TOF analysis. In particular, the mass spectrum of AgP4PEG$_{750}$ (Fig. 1b) shows a cluster of peaks centered at about 3640Da ($\overline{Mn}$ = 3615 Da, $\overline{Mw}$ = 3760 Da), with two distributions of peaks distribution having *m/z* values of 3018 + *n* 44 and 3034 + *n* 44, corresponding to the [M]Na^+ (§) and [M]K^+ (°) species, respectively.

The formation of the Ag^{II}P4PEG$_{750}$ complex can be justified by considering that the Ag^+ ion has a considerable affinity for nitrogen donor atoms [34] and that when Ag^+ interacts with the nitrogen atoms in the porphyrin cavity a lowering of the redox potential occurs. So, in the presence of an equivalent of silver ions in solution, the disproportion phenomenon is favoured, involving the formation of Ag^0 and the oxidation of Ag^+ to Ag^{++} and its insertion into the porphyrin cavity (Scheme 1, Step 2) [33,34].

Further evidence of the Ag-porphyrin complex formation was obtained by spectroscopic studies.

The UV–Vis spectrum of the H_2P4PEG$_{750}$ (continuous blue line,

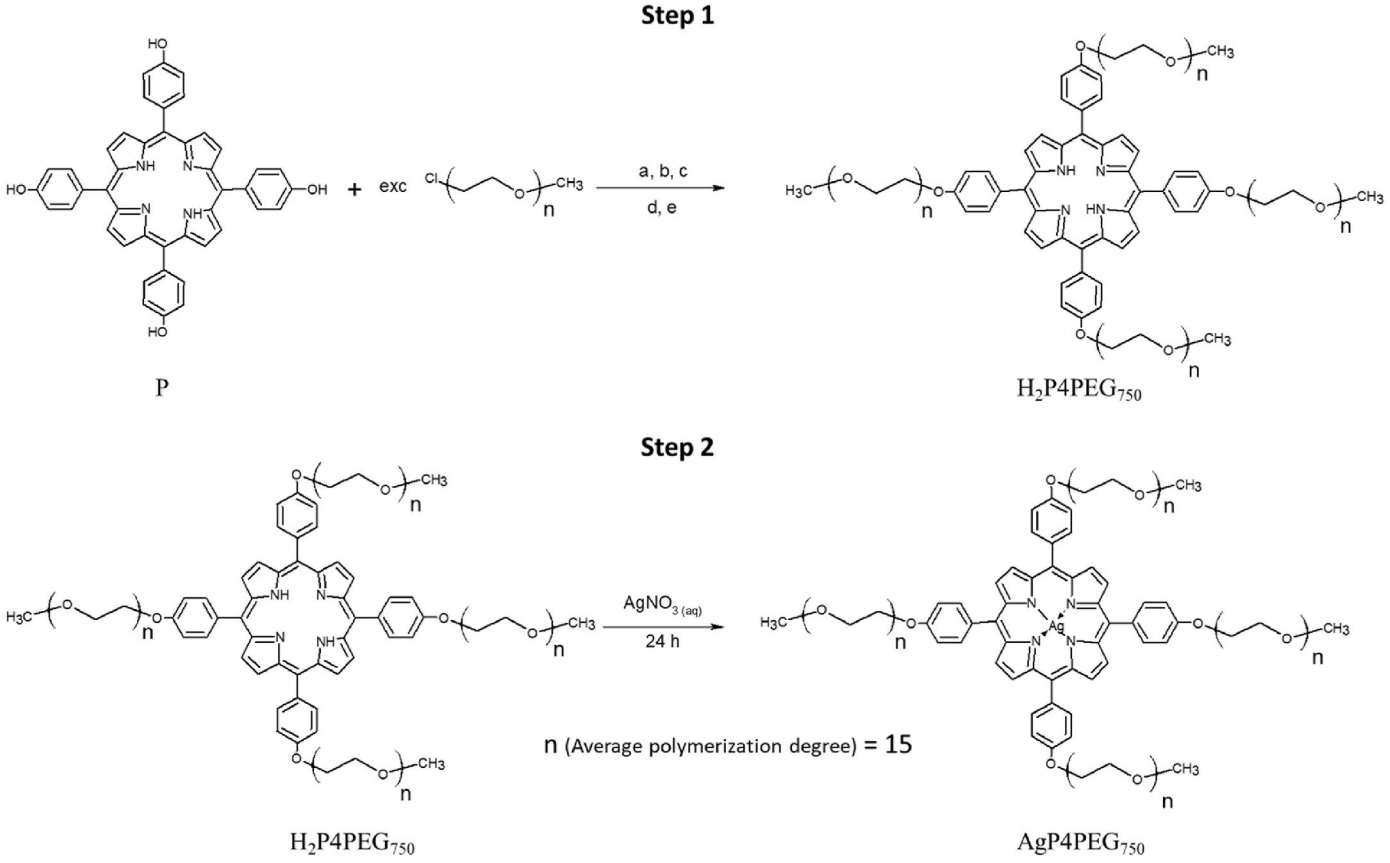

Scheme 1. Synthesis of H_2P4PEG$_{750}$ (Step 1) and AgP4PEG$_{750}$ (Step 2). a) PEGMEC$_{750}$ is dissolved in an H_2O/THF 1:1 mixture; b) P is dissolved in an aqueous solution of sodium hydroxide 0.5 M; c) the two solutions are mixed and refluxed for 76 h; d) the reaction product is acidified with acetic acid and dried under vacuum at 80 °C for 24 h; e) the residue is fractionated by column chromatography, H_2P4PEG$_{750}$ corresponds to the first eluted band (yield 30 %).

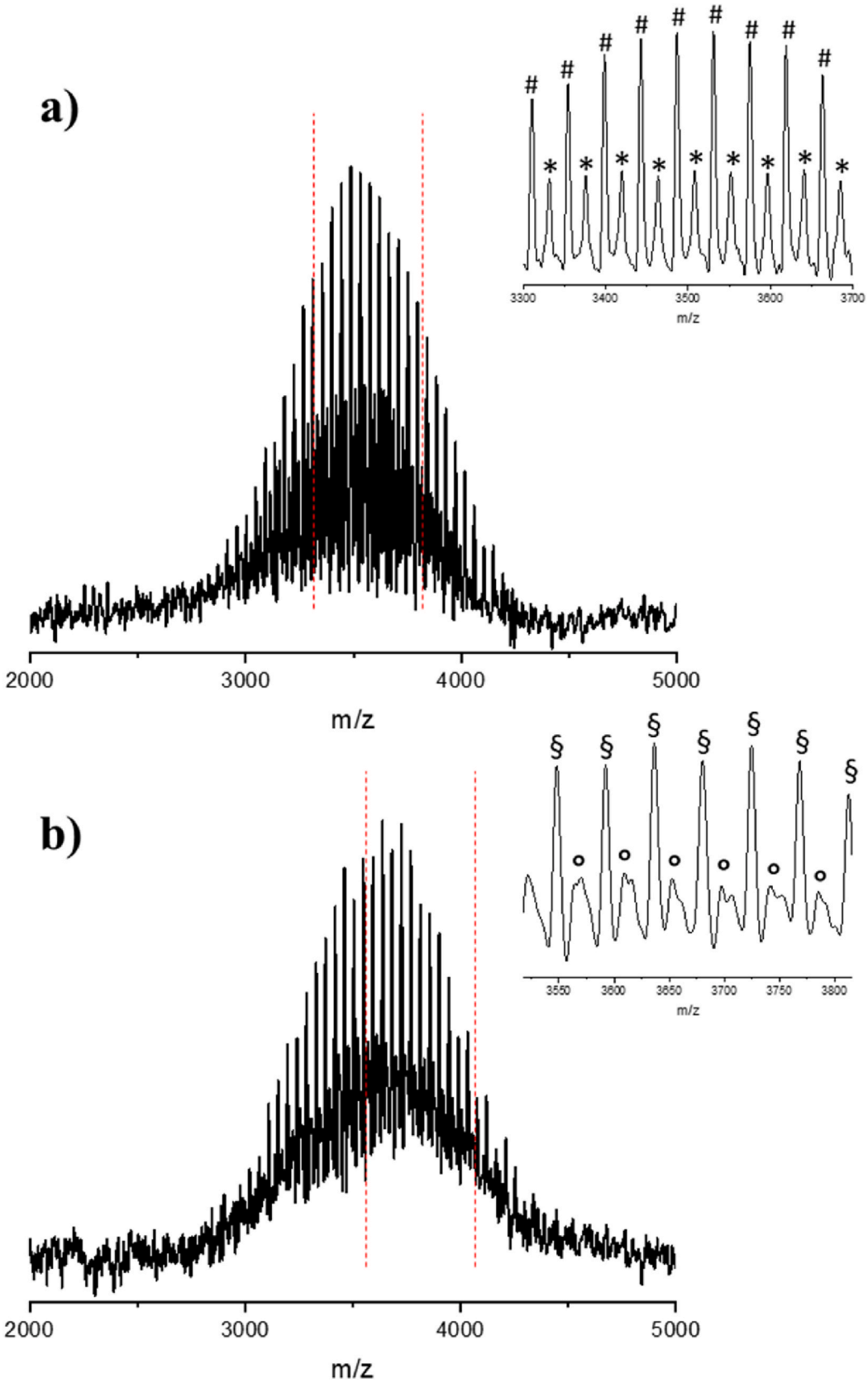

Fig. 1. MALDI-TOF mass spectra of P4PEG$_{750}$ (a) and AgP4PEG$_{750}$ (b). In inset: the magnification of the peaks included between the dashed red lines.

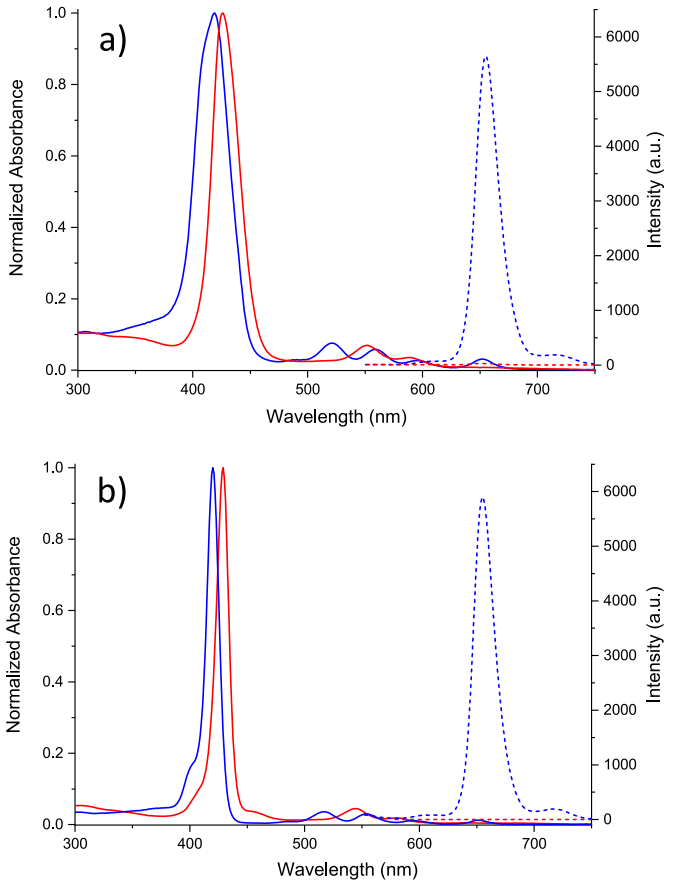

Fig. 2. UV–Vis (continuous line) and fluorescence (dashed line) spectra of H_2P4PEG_{750} (blue), $AgP4PEG_{750}$ (red) in water (a) and in THF (b).

Fig. 2a) shows a Soret band centered at 419 nm and four Q-bands at 520, 559, 596 and 652 nm (ε = 200,000 M^{-1} cm^{-1}), in line with the Gouterman four-orbital model [41].

The metalation with a silver ion of the H_2P4PEG_{750} determines a red shift of the Soret band at 426 nm (ε = 230,000 M^{-1} cm^{-1}), with the disappearance of the four Q-bands and the formation of two new unresolved Q-bands (continuous red line, Fig. 2a). Similar behavior occurs also in common organic solvents: using THF as the solvent, H_2P4PEG_{750} shows a Soret band at 420 nm and four Q-bands at 516, 554, 596 and 651 nm (continuous blue line, Fig. 2b), while $AgP4PEG_{750}$ shows the Soret band centered at 429 nm and two unresolved Q-bands (continuous red line, Fig. 2b).

Fluorescence emission spectra of H_2P4PEG_{750} both in water and THF (λ_{exc} at 435 nm, blue dashed lines, Fig. 2 a and b, respectively), show a strong fluorescence emission at 656 nm [32] at 655 nm, respectively.

Instead, the coordination of Ag ion in the porphyrinic core determines the quenching of the emission band at 656 nm (λ_{exc} 435 nm) in both water and THF solvents (dashed red lines in Fig. 2a and b).

3.2. Mechanisms of photo-demetallation of $AgP4PEG_{750}$

The $AgP4PEG_{750}$ combines the peculiar features of porphyrin [42] with that of silver ions [43], representing a potential multifunctional nanotool against a wide range of microorganisms. The unusual feature is attributed to the strain in the ligand frame caused by the size of the metal center. The metalloporphyrin with the silver (II) ion shows out-of-plane characteristics because the ionic radius of the metal center is too large to coplanarly fit into the cavity. In this case, the complex should display a photoredox activity undergoing photoinduced LMCT process [44] determining the reduction of the Silver ions and its exit from the porphyrin core, with the formation of free-porphyrin species.

To investigate the photo-demetallation phenomenon, occurring when the porphyrin is exposed to light irradiation, an aqueous solution of $AgP4PEG_{750}$ was irradiated with LED white light and monitored by UV–Vis and fluorescence spectroscopies (Fig. 3). Upon irradiation of $AgP4PEG_{750}$ a set of new Q bands (inset in Fig. 3, blue line) at λ = 516, 554, 596 and 651 nm was observed. Although the UV–Vis spectrum does not show a significative variation in correspondence of the Soret band, by exciting the solution at λ = 435 nm, differently to the starting solution of the $AgP4PEG_{750}$, the characteristic fluorescence spectrum of H_2P4PEG_{750} in water solution was observed (Fig. 3, dashed lines). In particular, the appearance of the signal at 652 nm, with the concomitant increase of the fluorescence intensity proves the restoration of the free porphyrin and the release of the Silver ions from the porphyrin core.

The experimental data suggest that the photoexcitation of the porphyrin is associated with the reduction of Ag^{++} ion with the formation of the $Ag^{I}HP4PEG_{750}$ (Scheme 2, eq. 1). The so-generated porphyrin reacts with water molecules in order to form the free-base porphyrin and Ag^{+} ion (Scheme 2, eq. 2). Accordingly, while the $AgP4PEG_{750}$ is not able to photo-generate singlet oxygen, a synergistic effect occurs with the release of Ag^{+} ions in solution (known to treat bacterial infections) [45] and the formation of H_2P4PEG_{750} (able to photo-generate singlet oxygen species) [23].

3.3. Photobactericidal activity

The photo-bactericidal activity of H_2P4PEG_{750} and $AgP4PEG_{750}$ has been established through biological assays against *P. aeruginosa* and *S. aureus*, among the most common pathogens involved in a wide range of infections, including severe and often fatal hospital-acquired infections.

The microbiological evaluation indicated good photobactericidal activity for all compounds, albeit to varying degrees (Fig. 4a and b). Otherwise, no significant bactericidal activity was detected when the same compounds were evaluated in dark conditions, suggesting that biocide activity was mainly due to the photoactivation of the porphyrin (Fig. 4c and d). Concerning *S. aureus,* no significant difference was observed among the evaluated compounds (Fig. 4a). Specifically, no visible growth of bacteria was detected when the concentration was equal to or greater than 6.25 μM. This concentration was also deduced as minimum bactericidal concentration (MBC) by sub-culturing in fresh medium (Table 1). Instead, data from *P. aeruginosa* showed that the photobactericidal activity of metalloporphyrin is always significantly reduced compared to H_2P4PEG_{750} (Fig. 4b). In this case, we observed no

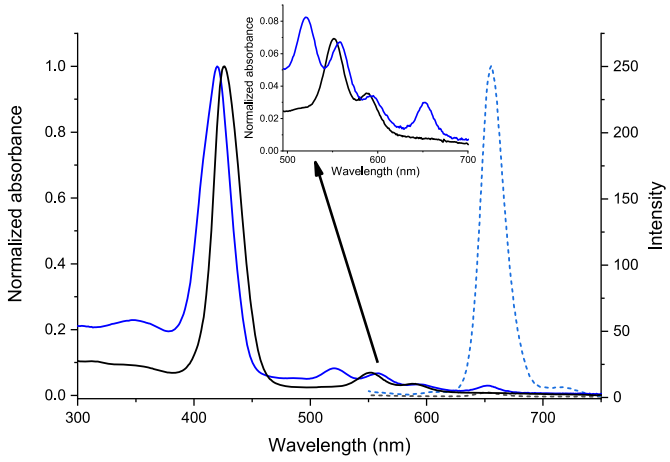

Fig. 3. UV-Vis (continuous lines) and fluorescence (dashed lines) changes before (black lines) and after 24 h photoirradiation (blue lines) of the $AgP4PEG_{750}$ in aqueous solution. In the inset, the magnification of the Q-bands wavelength range.

$$Ag^{II}P4PEG_{750} + H_2O \xrightarrow{h\nu} Ag^{I}HP4PEG_{750} + {}^{*}OH \quad (1)$$

$$Ag^{I}HP4PEG_{750} + H_2O \rightarrow H_2P4PEG_{750} + Ag^{+} + {}^{\cdot}OH \quad (2)$$

Scheme 2. Mechanism for the photoinduced demetallation of $AgP4PEG_{750}$.

visible growth for H_2P4PEG_{750} at a molar concentration of 12.5 μM, while for $AgP4PEG_{750}$ the absence of growth was located at 25 μM. As well as in this case, the values were confirmed as MBC (Table 1).

From antimicrobial assays, important deductions could be made about the evaluated compounds. Firstly, data indicated a higher susceptibility of the Gram-positive strain (*S. aureus*) compared to the Gram-negative one (*P. aeruginosa*) for the photo-activated porphyrins. The higher susceptibility of Gram-positive strain is due to its porous cell wall, mainly consisting of peptidoglycan and lipoteichoic acids and allowing diffusion of porphyrins to the intra-cellular target sites. Furthermore, the cell wall of Gram-negative strain, containing negatively charged lipopolysaccharide (LPS), hinders the passage of neutral (or also anionic) porphyrins from the external environment into bacterial cells [46].

Nevertheless, additional reports showed that the presence of electron-donating groups (i.e. PEG-OCH_3) induces the increase of the electron density on the pyrrole ring, which makes the porphyrin more basic and readily protonated. So, the systems having a greater positive charge are more in favor of absorption onto bacteria with a negative charged surface and likely produce more powerful biocidal activities against both Gram-positive and Gram-negative bacteria [47].

Referring to *P. aeruginosa,* the lower susceptibility of the strain allowed to discriminate the bactericidal activity when the silver ion was inserted into the core of the porphyrin. In particular, the data would suggest that upon irradiation, determining the demetallation of silver ions from the porphyrin core, only the amount of porphyrin without metal into its core could cause photo-bactericidal activity, whereas the part of porphyrin coordinated with silver ions could prevent this activity on bacterial strain.

Furthermore, the demetallation process could occur in different sites for the two pathogenic strains. Since the Gram-positive strain (*S. aureus*) has a more porous cell wall, both porphyrin and metalloporphyrin are able to easily reach the cytoplasm [48]. Following irradiation, the porphyrins produce ROS (e.g $^1O_2$), activating the redox pathways in *S. aureus*, such as bacilliredoxin/bacillithiol disulfide reductase, to maintain the reduced state of the cytoplasm [49]. The latter could increase the photo-demetallation of metalloporphyrins by easing the reduction of Ag^{2+} to Ag^{+} [29].

On the other hand, the release of Ag^{+} ions does not seem to improve the bactericidal properties, probably because Ag^{+} is under minimum inhibitory concentration (MIC) value. Otherwise, the Gram-negative strain (*P. aeruginosa*) would make the intracellular uptake of porphyrins more difficult, due to the outer lipopolysaccharide membrane. In this case, the demetallation process would be exclusively due to the photoreduction of the metalloporphyrin, resulting in slower and, in bactericidal terms, low effectiveness. In this case, the bactericidal effect of silver ions could be further reduced by phenazine pigments (e.g. pyocyanin, pyochelin, and pyoverdine), promoting the reduction of Ag^{+} to Ag^{0} [50]. In perspective, despite the low antibacterial activity of silver against the studied bacteria strains, the presence of silver ions in the

Table 1
MBC (μM) against *P. aeruginosa* and *S. aureus* under two different conditions at 37 °C, namely 4 h of White-Light Irradiation (Fluence 54.82 J/cm^2) and in the Dark.

*Compound	*S. aureus*		*P. aeruginosa*	
	MBC		MBC	
	Light	Dark	Light	Dark
H_2P4PEG_{750}	6.25	–	12.5	–
$AgP4PEG_{750}$	6.25	–	25	–

[a]The highest concentration carried out was 25 μM. The dashes correspond to a lack of activity below this concentration.

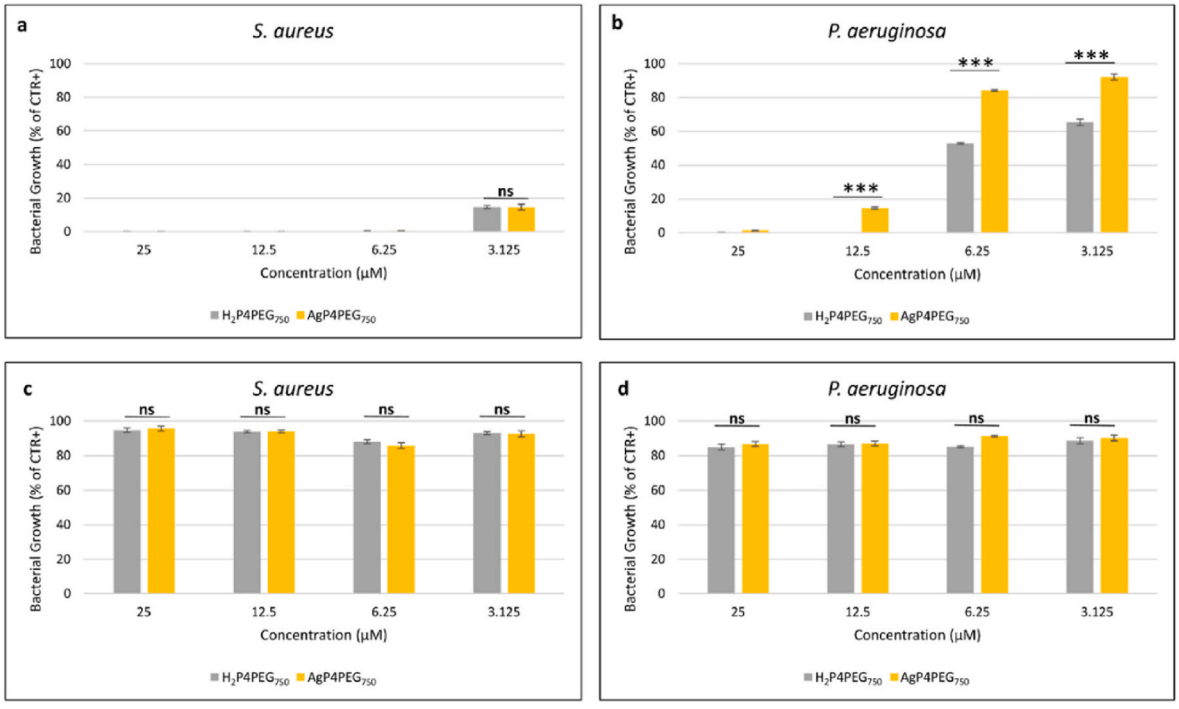

Fig. 4. Bacterial growth of *S. aureus* and *P. aeruginosa* in the presence of H_2P4PEG_{750} and $AgP4PEG_{750}$ after light exposition (a–b) by a white-LED source (total fluence 54.82 J/cm^2) and in the dark (*c*–d). Data, expressed as percentages compared to condition control (CTR, culture in the absence of any compound), represent mean ± SD for 3 replicates (n = 3). For the ANOVA test from Sidak's multiple comparisons test, one (*), two (**) and three (***) asterisks identify p-value <0.05, 0.01 and 0.001, respectively. Ns: not significant (see Tables S1–S2).

porphyrin cavity could allow the preservation of the porphyrin core from the spontaneous complexation of ions usually present in the biological environment [51] (Cu, Fe, etc.), which would make it inactive for the singlet oxygen generation. On the other hand, under light irradiation, the photodemetallation of silver-porphyrin is triggered, making it photoactive and acting as an antibacterial agent.

4. Conclusion

Herein, the synthesis and characterization of a PEGylated silver (II)-porphyrin system was reported. The experimental data suggest the occurrence of a redox process leading to the formation of an Ag^{II}P4-PEG_{750} complex. UV–Vis and fluorescence spectroscopies confirmed that under photoirradiation, with white LED light, a photodemetallation event occurs in water solution, causing the release of silver ions in solution and the recovery of the free-base PEGylated porphyrin. This phenomenon could also happen during the photoirradiation of dyes involved in *in-vitro* biological assays. The chemical-physical properties of the investigated systems result in different biological activity against gram-positive or gram-negative bacteria strains, due to different dye-uptake behavior. Despite the released Ag^{+} ions concentration might be under MIC value, the presence of the metal ion induces the different bactericidal activity of the photoactivated polymeric dyes. Moreover, the data suggest that only the free-base porphyrin shows photobactericidal activity. The interaction of the photoactivated metal-porphyrin derivative with the cytoplasmatic environment of Gram-positive bacteria could also support the demetallation of the system through selective redox pathways, resulting in the higher efficacy of the photobactericidal system. Finally, the presence of silver ions in the porphyrin cavity allows the preservation of the porphyrin core from the complexation of ions usually present in the biological environment [51] (Cu, Fe, etc.), which would make it inactive for singlet oxygen generation. Instead, under light irradiation, the photo-demetallation of silver-porphyrin makes it photoactive and can act as an antibacterial agent.

CRediT authorship contribution statement

Fabiana Vento: Data curation, Formal analysis, Writing – original draft, Writing – review & editing. **Angelo Nicosia:** Conceptualization, Data curation, Methodology, Project administration, Resources, Validation, Visualization, Writing – review & editing. **Lidia Mezzina:** Data curation, Formal analysis, Investigation, Resources, Visualization, Writing – review & editing. **Domenico Franco:** Data curation, Formal analysis, Investigation, Methodology, Validation, Visualization, Writing – original draft, Writing – review & editing. **Roberto Zagami:** Data curation, Formal analysis, Investigation, Methodology, Validation, Visualization, Writing – original draft, Writing – review & editing. **Antonino Mazzaglia:** Conceptualization, Data curation, Methodology, Resources, Supervision, Validation, Visualization, Writing – original draft, Writing – review & editing. **Placido Giuseppe Mineo:** Conceptualization, Funding acquisition, Methodology, Project administration, Resources, Supervision, Validation, Visualization, Writing – original draft, Writing – review & editing.

Declaration of competing interest

The authors declare that they have no known competing financial interests or personal relationships that could have appeared to influence the work reported in this paper.

Data availability

No data was used for the research described in the article.

Acknowledgements

The authors also acknowledged funding from the University of Catania (Piano di incentivi per la ricerca di Ateneo, Linea di Intervento 2 - Project MaMeX).

Appendix A. Supplementary data

Supplementary data to this article can be found online at https://doi.org/10.1016/j.dyepig.2024.111957.

References

[1] Medina Cruz D, Mi G, Webster TJ. Synthesis and characterization of biogenic selenium nanoparticles with antimicrobial properties made by Staphylococcus aureus, methicillin-resistant Staphylococcus aureus (MRSA), Escherichia coli, and Pseudomonas aeruginosa. J Biomed Mater Res 2018;106(5):1400–12. https://doi.org/10.1002/jbm.a.36347.
[2] Robinson DA, Griffith RW, Shechtman D, Evans RB, Conzemius MG. In vitro antibacterial properties of magnesium metal against Escherichia coli, Pseudomonas aeruginosa and Staphylococcus aureus. Acta Biomater 2010;6(5):1869–77. https://doi.org/10.1016/j.actbio.2009.10.007.
[3] Von Borowski RG, Trentin DS, Johnson KN. Biofilms and coronavirus reservoirs: a perspective review. Appl Environ Microbiol 2021;87(18). https://doi.org/10.1128/aem.00859-21.
[4] Pang Z, Raudonis R, Glick BR, Lin T-J, Cheng Z. Antibiotic resistance in Pseudomonas aeruginosa: mechanisms and alternative therapeutic strategies. Biotechnol Adv 2019;37(1):177–92. https://doi.org/10.1016/j.biotechadv.2018.11.013.
[5] Martin E, Lina G, Dumitrescu O. STAPHYLOCOCCUS | Staphylococcus aureus. In: Encyclopedia of food microbiology. second ed. Academic Press; 2014. p. 501–7.
[6] Serra R, Grande R, Butrico L, Rossi A, Settimio UF, Caroleo B, et al. Chronic wound infections: the role of Pseudomonas aeruginosa and Staphylococcus aureus. Expert Rev Anti-infect Ther 2015;13(5):605–13. https://doi.org/10.1586/14787210.2015.1023291.
[7] Orazi G, O'Toole GA, Dunman P. Pseudomonas aeruginosa alters Staphylococcus aureus sensitivity to vancomycin in a biofilm model of cystic fibrosis infection. mBio 2017;8(4). https://doi.org/10.1128/mBio.00873-17.
[8] Cho J-A, Roh YJ, Son HR, Choi H, Lee J-W, Kim SJ, et al. Assessment of the biofilm-forming ability on solid surfaces of periprosthetic infection-associated pathogens. Sci Rep 2022;12(1). https://doi.org/10.1038/s41598-022-22929-z.
[9] Chambers HF, DeLeo FR. Waves of resistance: Staphylococcus aureus in the antibiotic era. Nat Rev Microbiol 2009;7(9):629–41. https://doi.org/10.1038/nrmicro2200.
[10] Bryers JD, Jarvis RA, Lebo J, Prudencio A, Kyriakides TR, Uhrich K. Biodegradation of poly(anhydride-esters) into non-steroidal anti-inflammatory drugs and their effect on Pseudomonas aeruginosa biofilms in vitro and on the foreign-body response in vivo. Biomaterials 2006;27(29):5039–48. https://doi.org/10.1016/j.biomaterials.2006.05.034.
[11] Nicosia A, Vento F, Pellegrino AL, Ranc V, Piperno A, Mazzaglia A, et al. Polymer-based graphene derivatives and microwave-assisted silver nanoparticles decoration as a potential antibacterial agent. Nanomaterials 2020;10(11). https://doi.org/10.3390/nano10112269.
[12] Chopra I. The increasing use of silver-based products as antimicrobial agents: a useful development or a cause for concern? J Antimicrob Chemother 2007;59(4):587–90. https://doi.org/10.1093/jac/dkm006.
[13] Leid JG, Ditto AJ, Knapp A, Shah PN, Wright BD, Blust R, et al. In vitro antimicrobial studies of silver carbene complexes: activity of free and nanoparticle carbene formulations against clinical isolates of pathogenic bacteria. J Antimicrob Chemother 2011;67(1):138–48. https://doi.org/10.1093/jac/dkr408.
[14] Lemire JA, Harrison JJ, Turner RJ. Antimicrobial activity of metals: mechanisms, molecular targets and applications. Nat Rev Microbiol 2013;11(6):371–84. https://doi.org/10.1038/nrmicro3028.
[15] Zhang H, Li Q, Qi X, Li Y, Ma H, Grinholc M, et al. Iron-blocking antibacterial therapy with cationic heme-mimetic gallium porphyrin photosensitizer for combating antibiotic resistance and enhancing photodynamic antibacterial activity. Chem Eng J 2023:451. https://doi.org/10.1016/j.cej.2022.138261.
[16] Villari V, Micali N, Nicosia A, Mineo P. Water-soluble non-ionic PEGylated porphyrins: a versatile category of dyes for basic science and applications. Top Curr Chem 2021;379(5). https://doi.org/10.1007/s41061-021-00348-4.
[17] Mineo P, Faggio C, Micali N, Scamporrino E, Villari V. A star polymer based on a polyethylene glycol with a porphyrinic core as a photosensitizing agent for application in photodynamic therapy: tests in vitro on human erythrocytes. RSC Adv 2014;4(37). https://doi.org/10.1039/c3ra47913g.
[18] Stojiljkovic I, Evavold BD, Kumar V. Antimicrobial properties of porphyrins. Expet Opin Invest Drugs 2005;10(2):309–20. https://doi.org/10.1517/13543784.10.2.309.
[19] Oyim J, Omolo CA, Amuhaya EK. Photodynamic antimicrobial chemotherapy: advancements in porphyrin-based photosensitize development. Front Chem 2021;9. https://doi.org/10.3389/fchem.2021.635344.

[20] Vera C, Tulli F, Borsarelli CD. Photosensitization with supramolecular arrays for enhanced antimicrobial photodynamic treatments. Front Bioeng Biotechnol 2021; 9. https://doi.org/10.3389/fbioe.2021.655370.
[21] Zagami R, Rubin Pedrazzo A, Franco D, Caldera F, De Plano LM, Trapani M, et al. Supramolecular assemblies based on polymeric cyclodextrin nanosponges and a cationic porphyrin with antimicrobial photodynamic therapy action. Int J Pharm 2023:637. https://doi.org/10.1016/j.ijpharm.2023.122883.
[22] Beyene BB, Mihirteu AM, Ayana MT, Yibeltal AW. Synthesis, characterization and antibacterial activity of metalloporphyrins: role of central metal ion. Results in Chemistry 2020;2.
[23] Nicosia A, Vento F, Satriano C, Villari V, Micali N, Cucci LM, et al. Light-triggered polymeric nanobombs for targeted cell death. ACS Appl Nano Mater 2020;3(2): 1950–60. https://doi.org/10.1021/acsanm.9b02552.
[24] Chung CY-S, Fung S-K, Tong K-C, Wan P-K, Lok C-N, Huang Y, et al. A multi-functional PEGylated gold(iii) compound: potent anti-cancer properties and self-assembly into nanostructures for drug co-delivery. Chem Sci 2017;8(3):1942–53. https://doi.org/10.1039/c6sc03210a.
[25] Sibrian-Vazquez M, Jensen TJ, Vicente MGH. Synthesis and cellular studies of PEG-functionalized meso-tetraphenylporphyrins. J Photochem Photobiol B Biol 2007;86 (1):9–21. https://doi.org/10.1016/j.jphotobiol.2006.08.004.
[26] Mineo PG, Abbadessa A, Rescifina A, Mazzaglia A, Nicosia A, Scamporrino AA. PEGylate porphyrin-gold nanoparticles conjugates as removable pH-sensor nano-probes for acidic environments. Colloids Surf A Physicochem Eng Asp 2018;546: 40–7. https://doi.org/10.1016/j.colsurfa.2018.02.061.
[27] Waku T, Matsusaki M, Kaneko T, Akashi M. PEG brush peptide nanospheres with stealth properties and chemical functionality. Macromolecules 2007;40(17): 6385–92. https://doi.org/10.1021/ma0707638.
[28] Nicosia A, Abbadessa A, Vento F, Mazzaglia A, Mineo PG. Silver nanoparticles decorated with PEGylated porphyrins as potential theranostic and sensing agents. Materials 2021;14(11). https://doi.org/10.3390/ma14112764.
[29] Kunkely H, Vogler A. Photodemetalation of silver(II) tetraphenylporphyrin. Inorg Chem Commun 2007;10(4):479–81. https://doi.org/10.1016/j.inoche.2007.01.007.
[30] Villari V, Mineo P, Micali N, Angelini N, Vitalini D, Scamporrino E. Uncharged water-soluble porphyrin tweezers as a supramolecular sensor for α-amino acids. Nanotechnology 2007;18(37). https://doi.org/10.1088/0957-4484/18/37/375503.
[31] Mineo P, Scamporrino E, Vitalini D. Synthesis and characterization of uncharged water-soluble star polymers containing a porphyrin core. Macromol Rapid Commun 2002;23(12):681–7. https://doi.org/10.1002/1521-3927(20020801)23:12<681::Aid-marc681>3.0.Co;2-i.
[32] Mineo PG, Vento F, Abbadessa A, Scamporrino E, Nicosia A. An optical sensor of acidity in fuels based on a porphyrin derivative. Dyes Pigments 2019;161:147–54. https://doi.org/10.1016/j.dyepig.2018.09.045.
[33] Atoyebi AO, Brückner C. Observations on the mechanochemical insertion of zinc (II), copper(II), magnesium(II), and select other metal(II) ions into porphyrins. Inorg Chem 2019;58(15):9631–42. https://doi.org/10.1021/acs.inorgchem.9b00052.
[34] Brückner C. The silver complexes of porphyrins, corroles, and carbaporphyrins: silver in the oxidation states II and III. J Chem Educ 2004;81(11). https://doi.org/10.1021/ed081p1665.
[35] Zagami R, Franco D, Pipkin JD, Antle V, De Plano L, Patanè S, et al. Sulfobutylether-β-cyclodextrin/5,10,15,20-tetrakis(1-methylpyridinium-4-yl) porphine nanoassemblies with sustained antimicrobial phototherapeutic action. Int J Pharm 2020;585. https://doi.org/10.1016/j.ijpharm.2020.119487.
[36] Vitalini D, Mineo P, Scamporrino E. Effect of combined changes in delayed extraction time and potential gradient on the mass resolution and ion discrimination in the analysis of polydisperse polymers and polymer blends by delayed extraction matrix-assisted laser desorption/ionization time-of-flight mass spectrometry. Rapid Commun Mass Spectrom 1999;13(24):2511–7. https://doi.org/10.1002/(sici)1097-0231(19991230)13:24<2511::Aid-rcm819>3.0.Co;2-y.
[37] Mineo P, Vitalini D, Scamporrino E, Bazzano S, Alicata R. Effect of delay time and grid voltage changes on the average molecular mass of polydisperse polymers and polymeric blends determined by delayed extraction matrix-assisted laser desorption/ionization time-of-flight mass spectrometry. Rapid Commun Mass Spectrom 2005;19(19):2773–9. https://doi.org/10.1002/rcm.2123.
[38] Scamporrino E, Vitalini D, Mineo P. Synthesis and MALDI-TOF MS characterization of high molecular weight poly(1,2-dihydroxybenzene phthalates) obtained by uncatalyzed bulk polymerization of O,O'-phthalid-3-ylidenecatechol or 4-methyl-O,O'-phthalid-3-ylidenecatechol. Macromolecules 1996;29(17):5520–8. https://doi.org/10.1021/ma960051+.
[39] Scamporrino E, Maravigna P, Vitalini D, Mineo P. A new procedure for quantitative correction of matrix-assisted laser desorption/ionization time-of-flight mass spectrometric response. Rapid Commun Mass Spectrom 1998;12(10):646–50. https://doi.org/10.1002/(sici)1097-0231(19980529)12:10<646::Aid-rcm208>3.0.Co;2-c.
[40] Godziela GM, Goff HM. Solution characterization of copper (II) and silver (II) porphyrins and the one-electron oxidation products by nuclear magnetic resonance spectroscopy. J Am Chem Soc 1986;108(9):2237–43. https://doi.org/10.1021/ja00269a019.
[41] Gouterman M, Wagnière GH, Snyder LC. Spectra of porphyrins. J Mol Spectrosc 1963;11(1–6):108–27. https://doi.org/10.1016/0022-2852(63)90011-0.
[42] Wang J, Zhang X, Liu Y, Wang Z, Wang P, Zheng Z, et al. Enhanced singlet oxygen production over a photocatalytic stable metal organic framework composed of porphyrin and Ag. J Colloid Interface Sci 2021;602:300–6. https://doi.org/10.1016/j.jcis.2021.05.087.
[43] Low WL, Martin C, Hill DJ, Kenward MA. Antimicrobial efficacy of silver ions in combination with tea tree oil against Pseudomonas aeruginosa, Staphylococcus aureus and Candida albicans. Int J Antimicrob Agents 2011;37(2):162–5. https://doi.org/10.1016/j.ijantimicag.2010.10.015.
[44] Horváth O, Valicsek Z, Harrach G, Lendvay G, Fodor MA. Spectroscopic and photochemical properties of water-soluble metalloporphyrins of distorted structure. Coord Chem Rev 2012;256(15–16):1531–45. https://doi.org/10.1016/j.ccr.2012.02.011.
[45] Bjarnsholt T, Kirketerp-Møller K, Kristiansen S, Phipps R, Nielsen AK, Jensen PØ, et al. Silver against Pseudomonas aeruginosa biofilms. Apmis 2007;115(8):921–8. https://doi.org/10.1111/j.1600-0463.2007.apm_646.x.
[46] Amos-Tautua B, Songca S, Oluwafemi O. Application of porphyrins in antibacterial photodynamic therapy. Molecules 2019;24(13). https://doi.org/10.3390/molecules24132456.
[47] Wang J, Yang X, Song H, Liao W, Zhuo L, Wang G, et al. Visible light-induced biocidal activities and mechanistic study of neutral porphyrin derivatives against S. aureus and E. coli. J Photochem Photobiol B Biol 2018;185:199–205. https://doi.org/10.1016/j.jphotobiol.2018.06.003.
[48] Liu Y, Qin R, Zaat SAJ, Breukink E, Heger M. Antibacterial photodynamic therapy: overview of a promising approach to fight antibiotic-resistant bacterial infections. J Clin Transl Res 2015;1(3):140–67. https://doi.org/10.18053/jctres.201503.002.
[49] Linzner N, Loi VV, Fritsch VN, Tung QN, Stenzel S, Wirtz M, et al. Staphylococcus aureus uses the bacilliredoxin (BrxAB)/Bacillithiol disulfide reductase (YpdA) redox pathway to defend against oxidative stress under infections. Front Microbiol 2019;10. https://doi.org/10.3389/fmicb.2019.01355.
[50] Ellis DH, Maurer-Gardner EI, Sulentic CEW, Hussain SM. Silver nanoparticle antibacterial efficacy and resistance development in key bacterial species. Biomedical Physics & Engineering Express 2018;5(1). https://doi.org/10.1088/2057-1976/aad5a7.
[51] Sommer S, Rimington C, Moan J. Formation of metal complexes of tumor-localizing porphyrins. FEBS (Fed Eur Biochem Soc) Lett 2001;172(2):267–71. https://doi.org/10.1016/0014-5793(84)81138-2.